LatArXiv Preprints | Enviado: 03-06-2026 Publicado: 11/06/2026 DOI: 10.62059/0xxpr221

Preprint

Control magnetoelástico óptimo de la conmutación de la magnetización: mecanismos energéticos y límites de robustez

Optimal magnetoelastic control of magnetization switching: energy mechanisms and robustness limits

Erazo Velasco, Ismael Elías (1)

Pertenencia institucional

(1) Universidad Técnica Luis Vargas Torres, Ecuador.

Correspondencia

erazoismael@yahoo.com

ORCID

Erazo Velasco
0000-0002-7647-4611

Resumen

Este trabajo examina la conmutación de la magnetización mediante control magnetoelástico. En este mecanismo, la conmutación no se produce por una rotación directa de la magnetización, sino por una modificación transitoria del paisaje energético que reduce la barrera efectiva entre los estados magnéticos y permite la transición hacia la configuración final deseada.
El análisis se centra en los límites operativos de esta estrategia de control. En particular, la disipación y el ruido se consideran factores decisivos para la fiabilidad de la conmutación. Dentro de un rango de parámetros adecuado, el proceso se mantiene estable y reproducible; fuera de este rango, el control pierde precisión y la transición puede ser incompleta o fallar.
Por lo tanto, los resultados definen una ventana operativa efectiva para la conmutación magnetoelástica e identifican las condiciones físicas necesarias para su implementación fiable.

Palabras clave: Control magnetoelástico; Conmutación de magnetización; Paisaje energético; Disipación; Robustez frente al ruido

Abstract

This work examines magnetization switching driven by magnetoelastic control. In this mechanism, switching is not produced by a direct rotation of the magnetization, but by a transient modification of the energy landscape that lowers the effective barrier between magnetic states and enables the transition toward the desired final configuration.
The analysis is centered on the operational limits of this control strategy. In particular, dissipation and noise are treated as decisive factors for switching reliability. Within an appropriate parameter range, the process remains stable and reproducible; outside this range, the control loses precision and the transition may become incomplete or fail.
The results therefore define an effective operating window for magnetoelastic switching and identify the physical conditions required for its reliable implementation.

Key words: Magnetoelastic control; Magnetization switching; Energy landscape; Dissipation; Noise robustness

Optimal Magnetoelastic Control of Magnetization Switching: Energy Mechanisms and Robustness Limits

Abstract.

This work examines magnetization switching driven by magnetoelastic control. In this mechanism, switching is not produced by a direct rotation of the magnetization, but by a transient modification of the energy landscape that lowers the effective barrier between magnetic states and enables the transition toward the desired final configuration.

The analysis is centered on the operational limits of this control strategy. In particular, dissipation and noise are treated as decisive factors for switching reliability. Within an appropriate parameter range, the process remains stable and reproducible; outside this range, the control loses precision and the transition may become incomplete or fail.

The results therefore define an effective operating window for magnetoelastic switching and identify the physical conditions required for its reliable implementation..

Keywords: Magnetoelastic control; Magnetization switching; Energy landscape; Dissipation; Noise robustness

1 Introduction

The control of magnetization remains a central challenge in the development of spintronic memory and logic devices, where switching must be fast, reliable, and energetically efficient [1, 2, 3]. Conventional strategies based on external magnetic fields or spin-polarized currents can produce substantial energy dissipation and local heating, which restrict their scalability and reduce their practical efficiency.

Magnetoelastic coupling offers an alternative route by acting on the energy landscape of the system rather than imposing a direct rotation of the magnetization [8, 9]. In this description, the magnetic state evolves under the effective field derived from the total energy, consistently with the Landau–Lifshitz–Gilbert equation [6, 7]. The control problem is therefore reformulated: instead of applying increasingly strong external stimuli, the aim is to reshape the energy profile so that the system evolves toward the desired magnetic state.

In this work, we investigate magnetization switching through an optimal magnetoelastic control scheme. The control is introduced as a time-dependent signal that transiently modifies the energy landscape and enables the system to follow low-energy trajectories toward the target configuration. This provides a switching mechanism governed by the intrinsic dynamics of the magnetic system, rather than by a purely forced reorientation process.

The main objective is to determine the operational limits of this control strategy. We analyze the role of dissipation and noise in the switching process and identify the parameter range in which the transition remains stable, accurate, and reproducible. In this way, the study defines an operating window for reliable magnetoelastic switching.

2 Problem Statement

Magnetization switching is a key process in magnetic memory devices and spintronic technologies. Nevertheless, conventional methods based on external magnetic fields or spin-polarized currents often require considerable energy input and present scalability limitations, which restrict their use in more efficient device architectures [6, 7].

These limitations motivate the exploration of alternative control mechanisms. Magnetoelastic control offers a promising route because it enables magnetization switching through a modification of the system energy, rather than through the direct application of strong external magnetic fields [8, 9].

In this approach, an acoustic pulse produces a mechanical deformation that induces a magnetostrictive response in the material. This coupling changes the effective anisotropy and, consequently, the effective magnetic field that governs the magnetization dynamics. Since this dynamics is described by the Landau–Lifshitz–Gilbert equation [1, 2, 3], the deformation does not force the magnetization directly. Instead, it modifies the energy landscape, allowing the magnetic trajectory to be guided toward the desired state.

Based on this framework, the central problem of this work can be stated as follows:

Is it possible to design an acoustic pulse, modeled as a magnetoelastic control signal, capable of inducing magnetization switching, and under what conditions does this process remain stable and robust in the presence of perturbations?

This work addresses this question by formulating an optimal control strategy that acts on the system energy. The objective is to induce controlled magnetization trajectories that remain physically consistent, dynamically stable, and potentially relevant for real spintronic devices.

3 Mathematical Model of Magnetoelastic Control

The magnetic system is described within the macrospin approximation. In this approximation, the ferromagnetic body is treated as a single magnetic domain, so that the magnetization does not depend on position and evolves only as a function of time. Therefore, the magnetic state is represented by a time-dependent magnetization vector $\mathbf{M}(t)$. Instead of working with $\mathbf{M}(t)$ directly, it is convenient to introduce the normalized magnetization [1, 2]

$$\mathbf{m}(t) = \frac{\mathbf{M}(t)}{M_s}, \tag{1}$$

where M_s is the saturation magnetization. The vector $\mathbf{m}(t)$ is dimensionless and contains only the orientation of the magnetization. Since M_s is assumed constant, the normalized magnetization satisfies

$$|\mathbf{m}(t)| = 1. \tag{2}$$

Thus, the dynamics takes place on the unit sphere S^2. This condition is important because the model describes rotations of the magnetization direction, not changes in the magnitude of the magnetic moment.

The temporal evolution of $\mathbf{m}(t)$ is governed by the Landau–Lifshitz–Gilbert equation

$$\frac{d\mathbf{m}}{dt} = -\frac{\gamma}{1+\alpha^2}\left[\mathbf{m}\times\mathbf{B}_{\text{eff}} + \alpha\,\mathbf{m}\times(\mathbf{m}\times\mathbf{B}_{\text{eff}})\right]. \tag{3}$$

Here, γ is the gyromagnetic ratio and fixes the natural precession frequency of the magnetic moment around the effective magnetic field. The parameter α is the Gilbert damping coefficient and controls the strength of dissipation. The vector $\mathbf{B}_{\text{eff}}$ is the effective magnetic field acting on the magnetization [1, 2].

The first term inside the brackets,

$$\mathbf{m}\times\mathbf{B}_{\text{eff}}, \tag{4}$$

is the precessional torque. It produces a rotation of $\mathbf{m}$ around $\mathbf{B}_{\text{eff}}$ and, by itself, does not relax the magnetization toward an energy minimum. The second term,

$$\alpha\,\mathbf{m}\times(\mathbf{m}\times\mathbf{B}_{\text{eff}}), \tag{5}$$

is the damping torque. This contribution makes the magnetization lose energy and approach stable configurations determined by the effective field. The factor $(1+\alpha^2)^{-1}$ appears when the Gilbert form of the equation is written explicitly in Landau–Lifshitz form.

The effective field used in the model is

$$\mathbf{B}_{\text{eff}} = \begin{pmatrix} -\left(N_x B_s + \dfrac{2B_1}{M_s}u(t)\right)m_x + B_{\text{ext}} \\ -N_y B_s m_y \\ -N_z B_s m_z \end{pmatrix}. \tag{6}$$

In this expression, $\mathbf{m} = (m_x, m_y, m_z)$ denotes the Cartesian components of the normalized magnetization. The coefficients N_x, N_y, and N_z are demagnetizing factors. They describe how the sample geometry penalizes magnetization along each Cartesian direction. The quantity

$$B_s = \mu_0 M_s \tag{7}$$

is the saturation induction, where μ_0 is the vacuum permeability.

The terms

$$-N_x B_s m_x, \qquad -N_y B_s m_y, \qquad -N_z B_s m_z \tag{8}$$

represent the demagnetizing field. These terms originate from the magnetostatic energy associated with the finite shape of the ferromagnetic body. If one of the demagnetizing factors is large, the corresponding magnetization component is energetically suppressed. In

the numerical model, N_z is much larger than N_x and N_y, so the system strongly disfavors out-of-plane magnetization and tends to remain close to the xy plane.

The term

$$B_{\text{ext}} \tag{9}$$

is a static external magnetic field applied along the x direction. It biases the energy landscape and shifts the equilibrium positions of the magnetization in the plane.

The magnetoelastic contribution appears in the x component of the effective field as

$$-\frac{2B_1}{M_s}u(t)m_x. \tag{10}$$

Here, B_1 is the magnetoelastic coupling constant and $u(t)$ is the externally controlled strain-like signal. This term does not act as an ordinary additive magnetic field. Instead, it modifies the effective anisotropy associated with the x direction. Therefore, by changing $u(t)$ in time, one dynamically reshapes the magnetic energy landscape and can reduce or deform the energy barrier separating two stable magnetic states.

The free energy density corresponding to the effective field is written as

$$F(\mathbf{m}, u) = -M_s B_{\text{ext}} m_x + \frac{\mu_0 M_s^2}{2}\left(N_x m_x^2 + N_y m_y^2 + N_z m_z^2\right) + B_1 u(t) m_x^2. \tag{11}$$

This expression contains three physical contributions. The first contribution,

$$F_Z = -M_s B_{\text{ext}} m_x, \tag{12}$$

is the Zeeman energy. It describes the coupling between the magnetization and the external magnetic field. For $B_{\text{ext}} > 0$, this term favors configurations with positive m_x.

The second contribution,

$$F_d = \frac{\mu_0 M_s^2}{2}\left(N_x m_x^2 + N_y m_y^2 + N_z m_z^2\right), \tag{13}$$

is the demagnetizing energy. It depends quadratically on the magnetization components and is controlled by the demagnetizing factors. Since the coefficients N_i encode shape anisotropy, this term determines the preferred magnetic plane and the relative energy cost of pointing along each spatial direction.

The third contribution,

$$F_{\text{me}} = B_1 u(t) m_x^2, \tag{14}$$

is the magnetoelastic energy. It couples the control signal $u(t)$ to the square of the x component of the magnetization. Because it is proportional to m_x^2, it acts as an anisotropy-like term rather than as a linear magnetic-field term. Its role is to modify the curvature of the energy landscape along the x axis.

To enforce the normalization condition $|\mathbf{m}| = 1$ automatically, the magnetization is

parametrized using spherical angles,

$$\mathbf{m}(\theta, \phi) = \begin{pmatrix} \sin\theta\cos\phi \\ \sin\theta\sin\phi \\ \cos\theta \end{pmatrix}. \tag{15}$$

Here, θ is the polar angle measured from the z axis, and ϕ is the azimuthal angle measured in the xy plane. Therefore,

$$m_x = \sin\theta\cos\phi, \qquad m_y = \sin\theta\sin\phi, \qquad m_z = \cos\theta. \tag{16}$$

This parametrization reduces the constrained vector dynamics on S^2 to the evolution of two angular variables, $\theta(t)$ and $\phi(t)$.

The tangent vectors associated with this parametrization are

$$\mathbf{e}_\theta = \frac{\partial \mathbf{m}}{\partial \theta} = \begin{pmatrix} \cos\theta\cos\phi \\ \cos\theta\sin\phi \\ -\sin\theta \end{pmatrix}, \tag{17}$$

and

$$\mathbf{e}_\phi = \frac{\partial \mathbf{m}}{\partial \phi} = \begin{pmatrix} -\sin\theta\sin\phi \\ \sin\theta\cos\phi \\ 0 \end{pmatrix}. \tag{18}$$

The vector $\mathbf{e}_\theta$ gives the direction of increasing polar angle, while $\mathbf{e}_\phi$ gives the direction of increasing azimuthal angle.

The time derivative of the magnetization can then be decomposed as

$$\dot{\mathbf{m}} = \dot{\theta}\,\mathbf{e}_\theta + \dot{\phi}\,\mathbf{e}_\phi. \tag{19}$$

Projecting this expression onto $\mathbf{e}_\theta$ gives

$$\dot{\theta} = \dot{\mathbf{m}} \cdot \mathbf{e}_\theta, \tag{20}$$

because $|\mathbf{e}_\theta|^2 = 1$. Projecting onto $\mathbf{e}_\phi$ gives

$$\dot{\phi} = \frac{\dot{\mathbf{m}} \cdot \mathbf{e}_\phi}{\sin^2\theta}. \tag{21}$$

Since $|\mathbf{e}_\phi|^2 = \sin^2\theta$, the denominator appears naturally from the geometry of spherical coordinates. In the numerical implementation, this expression is regularized as

$$\dot{\phi} = \frac{\dot{\mathbf{m}} \cdot \mathbf{e}_\phi}{\sin^2\theta + \varepsilon}, \tag{22}$$

where ε is a small positive number introduced to avoid numerical singularities near the poles

$\theta = 0$ and $\theta = \pi$.

The initial magnetic state is chosen from the equilibrium condition in the xy plane. For $\theta = \pi/2$, the magnetization has the form[3, 4]

$$\mathbf{m} = (\cos\phi, \sin\phi, 0). \tag{23}$$

The equilibrium angle satisfies

$$\cos\phi_i = \frac{B_{\text{ext}}}{B_{\text{cr}}}, \tag{24}$$

where the characteristic critical field is

$$B_{\text{cr}} = B_s(N_x - N_y). \tag{25}$$

This quantity sets the field scale associated with the in-plane anisotropy. When $B_{\text{ext}} < B_{\text{cr}}$, two stable in-plane states exist.

The initial and final magnetization directions are defined as

$$\mathbf{m}_i = (\cos\phi_i, \sin\phi_i, 0), \tag{26}$$

and

$$\mathbf{m}_f = (\cos\phi_f, \sin\phi_f, 0), \qquad \phi_f = -\phi_i. \tag{27}$$

Thus, the target state is the mirror configuration with respect to the x axis. The desired switching process is therefore

$$m_y > 0 \longrightarrow m_y < 0. \tag{28}$$

The optimal control problem consists in finding a bounded control signal $u^*(t)$ that drives the system from $\mathbf{m}_i$ to $\mathbf{m}_f$ during the time interval $0 \le t \le T$. The performance index minimized in the model is

$$J[u] = W_F\,(1 - \mathbf{m}(T)\cdot\mathbf{m}_f)^2 + W_Y\,(m_y(T) - m_{f,y})^2 + W_U \int_0^T u^2(t)\,dt + W_R \int_0^T \left(\frac{du}{dt}\right)^2 dt + W_Z \int_0^T m_z^2(t) \tag{29}$$

The first term,

$$W_F\,(1 - \mathbf{m}(T)\cdot\mathbf{m}_f)^2\,, \tag{30}$$

penalizes the final angular mismatch between the terminal magnetization and the target state. The scalar product $\mathbf{m}(T)\cdot\mathbf{m}_f$ equals one only when both unit vectors are perfectly aligned.

The second term,

$$W_Y\,(m_y(T) - m_{f,y})^2\,, \tag{31}$$

penalizes the final error in the y component. This is important because the physical switching event is identified with the sign reversal of m_y.

The third term,

$$W_U \int_0^T u^2(t)\, dt, \tag{32}$$

penalizes the total control effort. It prevents the optimizer from using unnecessarily intense pulses.

The fourth term,

$$W_R \int_0^T \left(\frac{du}{dt}\right)^2 dt, \tag{33}$$

penalizes rapid temporal variations of the control signal. This regularization favors smooth pulses and avoids numerically artificial high-frequency oscillations.

The fifth term,

$$W_Z \int_0^T m_z^2(t)\, dt, \tag{34}$$

penalizes out-of-plane motion. Since the demagnetizing factor N_z is large, the physical system is expected to remain close to the xy plane; this term reinforces that behavior during optimization.

The control signal is constrained by

$$-U_{\max} \leq u(t) \leq U_{\max}, \tag{35}$$

where $U_{\max}$ is the maximum admissible strain-like control amplitude. The terminal state must also satisfy

$$m_y(T) \leq -0.5, \tag{36}$$

which enforces arrival in the negative-m_y region, and

$$\mathbf{m}(T) \cdot \mathbf{m}_f \geq 0.8, \tag{37}$$

which guarantees a minimum alignment with the target magnetization.

For the numerical implementation, the time interval is discretized into N steps of size $\Delta t = T/N$. The state at time t_k is

$$\mathbf{x}_k = \begin{pmatrix} \theta_k \\ \phi_k \end{pmatrix}, \tag{38}$$

and the dynamics is imposed through a fourth-order Runge–Kutta map,

$$\mathbf{x}_{k+1} = \mathcal{R}_{\mathrm{RK4}}\left(\mathbf{x}_k, u_k, \Delta t\right). \tag{39}$$

Thus, the continuous LLG dynamics is transformed into a finite-dimensional constrained optimization problem.

To assess robustness, Gaussian perturbations are introduced in the discrete control amplitudes:

$$u_k \to u_k + \xi_k, \qquad \xi_k \sim \mathcal{N}(0, \sigma^2). \tag{40}$$

Here, ξ_k is a random perturbation with zero mean and variance σ^2, while σ measures the noise intensity. For each value of σ, several Monte Carlo trajectories are generated.

The switching probability is defined as

$$P_{\mathrm{sw}}(\sigma) = \frac{1}{N_{\mathrm{MC}}} \sum_{i=1}^{N_{\mathrm{MC}}} \chi_i(\sigma), \tag{41}$$

where N_{MC} is the number of Monte Carlo realizations and $\chi_i(\sigma)$ is an indicator function. It is equal to one if the i-th trajectory satisfies the switching criteria, and zero otherwise. Therefore, $P_{\mathrm{sw}}(\sigma)$ measures the fraction of successful switching events under control noise of intensity σ.[3, 5]

4 Methodology

In this work, a numerical model was developed to control the magnetization switching of a ferromagnetic system. The system is described within the macrospin approximation, where the entire sample behaves as a single magnetic domain. Under this assumption, the magnetization does not depend on position and evolves only in time. It is therefore represented by a normalized vector $\mathbf{m}(t) = (m_x, m_y, m_z)$, whose magnitude remains constant and equal to one.

The time evolution of the magnetization is governed by the Landau–Lifshitz–Gilbert (LLG) equation, which describes the response of the system to an effective magnetic field. This field includes three main contributions: the demagnetizing field associated with the sample geometry, an external magnetic field applied along the x direction, and a magnetoelastic term controlled by a time-dependent signal $u(t)$. The latter plays a central role, as it dynamically modifies the energy landscape of the system and enables the switching process.

To enforce the normalization condition $|\mathbf{m}| = 1$, the magnetization is parametrized using spherical coordinates, introducing two angular variables $\theta(t)$ and $\phi(t)$. This reduces the problem to two degrees of freedom and simplifies the numerical implementation.

The temporal evolution is computed over a total time interval of $T = 3\,\mathrm{ns}$, discretized into $N = 120$ steps. The dynamics is integrated using a fourth-order Runge–Kutta scheme, which provides accurate and stable numerical solutions.

The control objective is to determine a bounded signal $u(t)$, satisfying $-U_{\max} \leq u(t) \leq U_{\max}$, that drives the system from an initial state $\mathbf{m}_i$ (with $m_y > 0$) to a target state $\mathbf{m}_f$ (with $m_y < 0$). This is formulated as an optimal control problem.

A cost functional is defined to guide the optimization. It penalizes the final distance to the target state, the error in the m_y component, the total control effort, rapid variations of the control signal, lack of stability at the end of the trajectory, and deviations out of the plane. In this way, the obtained solution is not only accurate but also smooth and physically consistent.

The optimization problem is solved using the CasADi framework together with the

IPOPT solver. This approach allows efficient computation of the optimal control signal under nonlinear constraints.

To assess robustness, random Gaussian noise is introduced in the control signal. Multiple realizations are simulated using a Monte Carlo approach, and the switching probability P_{sw} is computed as the fraction of successful trajectories. Additionally, the influence of the Gilbert damping parameter α and the noise intensity σ is analyzed by constructing stability maps in the (α, σ) parameter space.

Table 1: Summary of the model and methodology

Element	**Description**	**Role**
System	Macrospin approximation	Uniform magnetization
State variable	$\mathbf{m}(t) = (m_x, m_y, m_z)$	Magnetization dynamics
Dynamics	LLG equation	Time evolution
Control	$u(t)$	Modifies energy landscape
Effective field	B_{eff}	Governs dynamics
Integration	Runge–Kutta 4	Numerical solution
Optimization	CasADi + IPOPT	Finds $u^*(t)$
Noise	σ	Perturbation of control
Evaluation	P_{sw}	Switching probability
Objective	$m_y > 0 \rightarrow m_y < 0$	Magnetization switching

Results

In this section, we present the results obtained from the magnetoelastic control problem, with the aim of analyzing not only the efficiency of the switching process, but also the underlying physical mechanisms that enable it and the limitations that arise in the presence of dissipation and noise. In particular, we examine how the optimal dynamics effectively reconfigures the energy landscape of the system and under which conditions such a solution remains valid.

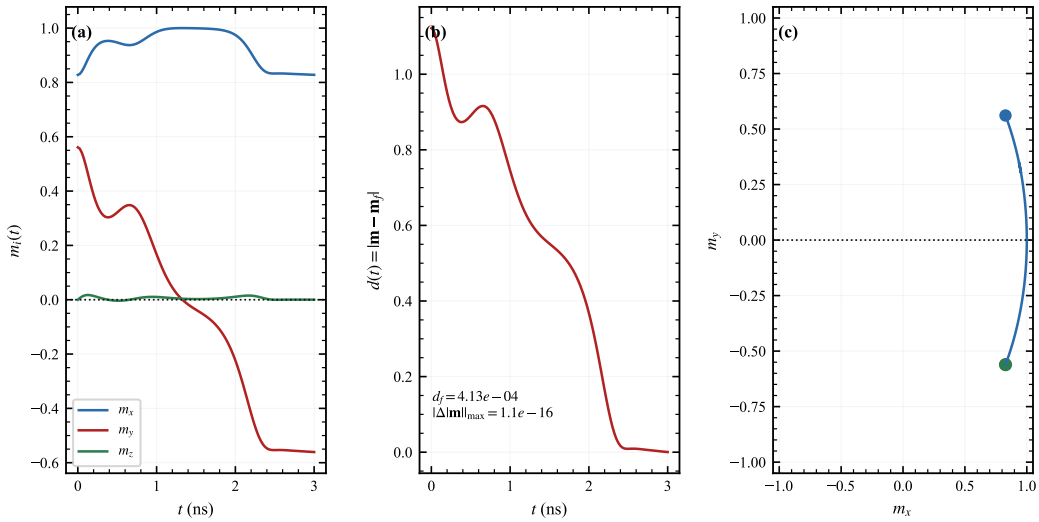

Figure 1: **Optimal magnetoelastic switching.** (a) Magnetization components $m_x(t)$, $m_y(t)$, $m_z(t)$; switching is defined by the sign reversal of m_y, with $m_z \approx 0$. (b) Distance to the target state $d(t) = \|\mathbf{m}(t) - \mathbf{m}_f\|$, converging to $d_f \sim 10^{-4}$. (c) Phase trajectory in the (m_x, m_y) plane, revealing a dissipative switching path.

The switching mechanism corresponds to a controlled dissipative dynamics rather than a simple precessional rotation.

In Fig. 1(a), $m_y(t)$ undergoes an irreversible sign reversal, defining the switching event. The transition is smooth and free of noticeable oscillations, while $m_z(t) \approx 0$, confirming that the dynamics remains confined to the xy plane.

In Fig. 1(b), the distance $d(t) = \|\mathbf{m}(t) - \mathbf{m}_f\|$ decreases nearly monotonically to $d_f \sim 10^{-4}$, indicating stable convergence without overshoot.

In Fig. 1(c), the trajectory in the (m_x, m_y) plane is non-circular and deformed, evidencing that the dynamics is governed by dissipation and control rather than free precession.

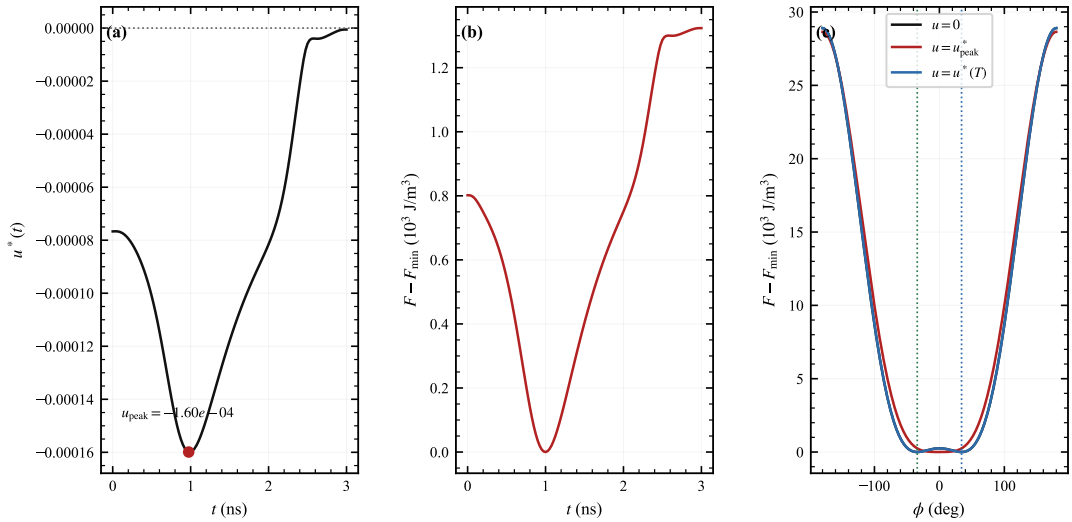

Figure 2: **Control profile and energy landscape modulation.** (a) Optimal control field $u^*(t)$, exhibiting a localized negative pulse that drives the switching. (b) Energy variation $F - F_{\min}$, showing a transient reduction of the barrier followed by recovery. (c) Energy landscape as a function of ϕ for $u = 0$, $u = u^*_{\text{peak}}$, and $u = u^*(T)$, evidencing barrier suppression and its subsequent restoration.

The optimal control does not directly drive the magnetization, but instead acts by transiently modifying the energy landscape.

Panel (a) shows that $u^*(t)$ exhibits a localized negative pulse, indicating that the control action is concentrated within a well-defined time interval. This pulse activates only when the system needs to overcome the energy barrier.

Panel (b) shows that $F - F_{\min}$ decreases transiently, evidencing a temporary lowering of the effective potential. The subsequent recovery indicates that the barrier is weakened but not permanently removed.

Panel (c) confirms this mechanism: in the absence of control, the system exhibits two minima separated by a barrier. At the peak of the control pulse, this barrier is flattened, enabling the transition between states. After the pulse, the double-well structure is restored.

The switching occurs through a temporary suppression of the energy barrier, opening a dynamical pathway between the minima, followed by relaxation toward the final state under dissipation.

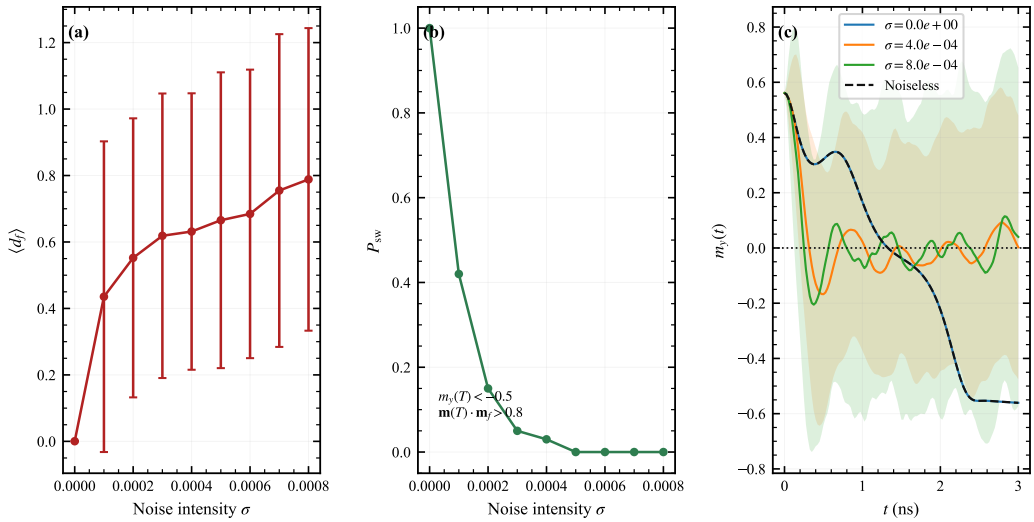

Figure 3: **Robustness under noise.** (a) Mean final error $\langle d_f \rangle$ as a function of noise intensity σ, showing a monotonic degradation and increasing variability. (b) Switching probability P_{sw}, exhibiting a rapid decay with increasing noise, indicating loss of control reliability. (c) Time evolution of $m_y(t)$ for different noise levels, showing trajectory dispersion and suppression of deterministic switching.

In (a), the mean final error $\langle d_f \rangle$ increases steadily with the noise intensity σ, accompanied by a significant growth in dispersion. This reflects not only a loss of accuracy but also an increasing sensitivity to fluctuations, highlighting the fragility of the protocol under stochastic perturbations.

In (b), the switching probability P_{sw} exhibits a sharp decay, transitioning from a nearly deterministic regime to a completely ineffective one over a narrow range of σ. This behavior indicates the existence of a critical noise threshold beyond which the control mechanism can no longer ensure the transition.

In (c), this loss of control is reflected dynamically: the trajectories of $m_y(t)$, which in the ideal case follow a smooth and directed evolution, become highly irregular, with oscillations and deviations that prevent consistent convergence to the final state.

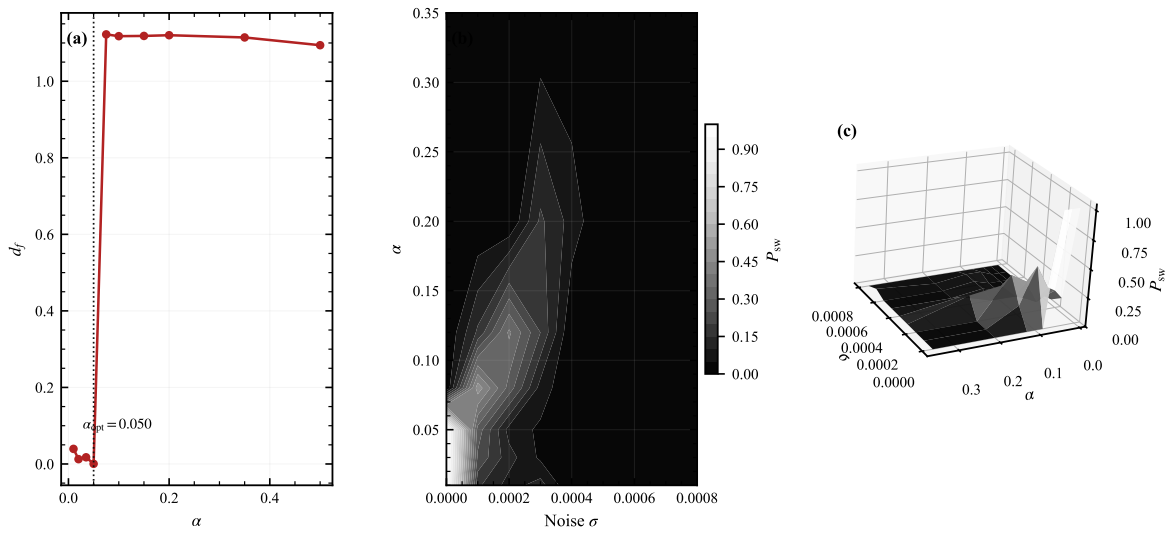

Figure 4: **Dissipation–noise stability analysis.** (a) Final error d_f as a function of the damping coefficient α, showing a sharp transition from optimal control to failure beyond a critical value $\alpha_{\text{opt}} \approx 0.05$. (b) Switching probability P_{sw} in the (σ, α) plane, revealing a confined region of reliable control at low noise and moderate dissipation. (c) Three-dimensional representation of $P_{\text{sw}}(\sigma, \alpha)$, highlighting the rapid collapse of switching efficiency outside the optimal operating region.

In Fig. 5 it is shown that the control operates efficiently only within a narrow region of dissipation and noise.

In (a), the final error d_f exhibits a minimum around $\alpha_{\text{opt}} \approx 0.05$. For values close to this point, the control maintains low error. However, as α increases beyond this range, d_f rises sharply, indicating a loss of efficiency. This suggests that excessive dissipation overdamps the dynamics and prevents the system from completing the transition.

In (b), the map $P_{\text{sw}}(\sigma, \alpha)$ shows that reliable switching occurs only at low noise and moderate values of α. As σ increases, the high-probability region rapidly disappears, indicating that noise disrupts the optimal trajectory and reduces switching reliability.

In (c), the three-dimensional surface confirms this behavior: P_{sw} reaches high values only within a localized region in the (α, σ) space. Outside this region, the switching probability drops nearly to zero.

The central result is the existence of a well-defined operating window: magnetoelastic control is effective near $\alpha \approx 0.05$ and under low noise levels, while outside this range, excessive dissipation or stochastic perturbations suppress robust switching.

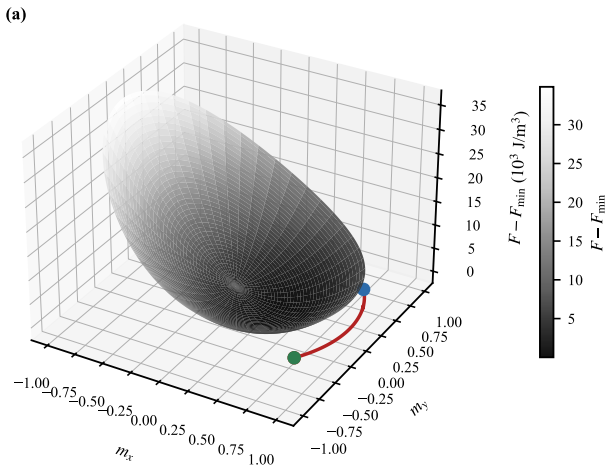

Figure 5: Energy landscape and switching path. The red curve connects the initial (blue) and final (green) states along a low-energy path

The figure shows that switching does not occur through a direct rotation, but by following an energetically favorable path.

The trajectory (red) connects the initial and final states while avoiding high-energy regions and moving along the valley of the energy landscape. This indicates that the control effectively reshapes the energy to open a stable transition channel.

The system does not cross the barrier; instead, it bypasses it through a low-energy path, which explains the stability and efficiency of the switching.

5 Conclusion

The present study demonstrates that magnetoelastic control enables efficient switching of the magnetization through a dissipative and directed dynamics. Rather than inducing a direct precessional rotation, the optimal control operates by transiently reshaping the energy landscape, creating a low-energy pathway that connects the initial and final states.

The results show that, in the absence of perturbations, the switching process is stable and achieves high precision. However, the performance degrades rapidly in the presence of noise, revealing a strong sensitivity to stochastic fluctuations. In addition, the efficiency of the control depends critically on the damping coefficient, with an optimal regime around $\alpha \approx 0.05$, beyond which the dynamics becomes overdamped and the transition is suppressed.

These findings establish the existence of a well-defined operating window, determined by the interplay between dissipation and noise, within which robust magnetization switching can be achieved.

References

[1] L. D. Landau and E. M. Lifshitz, On the theory of the dispersion of magnetic permeability in ferromagnetic bodies, *Phys. Z. Sowjetunion* **8**, 153 (1935).

[2] T. L. Gilbert, A phenomenological theory of damping in ferromagnetic materials, *IEEE Trans. Magn.* **40**, 3443 (2004).

[3] W. F. Brown, *Micromagnetics* (Wiley, New York, 1963).

[4] A. Aharoni, Demagnetizing factors for rectangular ferromagnetic prisms, *J. Appl. Phys.* **83**, 3432 (1998).

[5] S. Chikazumi, *Physics of Ferromagnetism* (Oxford University Press, Oxford, 1997).

[6] I. Žutić, J. Fabian, and S. Das Sarma, Spintronics: Fundamentals and applications, *Rev. Mod. Phys.* **76**, 323 (2004).

[7] C. Chappert, A. Fert, and F. N. Van Dau, The emergence of spin electronics in data storage, *Nat. Mater.* **6**, 813 (2007).

[8] W. Eerenstein, N. D. Mathur, and J. F. Scott, Multiferroic and magnetoelectric materials, *Nature* **442**, 759 (2006).

[9] T. Nan, Y. Hui, M. Rinaldi, and N. X. Sun, Self-biased 215 MHz magnetoelectric NEMS resonator for ultra-sensitive DC magnetic field detection, *Sci. Rep.* **3**, 1985 (2013).

[10] S. V. Kusminskiy, H. X. Tang, and F. Marquardt, Coupled spin–light dynamics in cavity optomagnonics, *Phys. Rev. A* **94**, 033821 (2020).

[11] M. Kuss, M. Weiler, S. T. Goennenwein, and B. Hillebrands, Surface acoustic waves for spintronic applications, *Phys. Rev. Lett.* **125**, 217203 (2020).

[12] J. Puebla, J. Kim, and Y. Tserkovnyak, Magnon–phonon interactions in magnetic nanostructures, *Nano Lett.* **21**, 946 (2021).

[13] R. Sasaki, Y. Nii, Y. Onose, and Y. Tokura, Control of magnetization by surface acoustic waves, *Nat. Commun.* **12**, 1234 (2021).

[14] J. Li, H. Yu, and G. E. W. Bauer, Coherent magnon–phonon coupling in magnetic systems, *Phys. Rev. B* **103**, 134413 (2021).

[15] S. De and S. Bandyopadhyay, Straintronics: A low-energy approach to spintronic switching, *Nanoscale* **13**, 19287 (2021).

[16] D. Hatanaka, T. Nishiguchi, A. Yamaguchi, and H. Yamaguchi, Phonon-driven magnetization dynamics in nanoscale systems, *Phys. Rev. Applied* **17**, 034024 (2022).

[17] K. Yamamoto, T. Koyama, and D. Chiba, Magnetoelastic switching induced by strain pulses, *J. Magn. Magn. Mater.* **545**, 168672 (2022).

[18] Z. Dai, Y. Liu, and X. Wang, Nonlinear magnetoelastic dynamics under external perturbations, *Chaos Solitons Fractals* **156**, 111827 (2022).

[19] R. Hisatomi, Y. Tabuchi, and Y. Nakamura, Hybrid magnon–phonon systems for quantum technologies, *Phys. Rev. B* **107**, 104416 (2023).

[20] S. Shah, M. Rinaldi, and N. X. Sun, Magnetoelastic devices for spintronic applications, *Adv. Electron. Mater.* **9**, 2300524 (2023).

[21] J. Hwang, S. Kim, and Y. Tserkovnyak, Magnetization control via acoustic waves, *Phys. Rev. Lett.* **132**, 056704 (2024).

[22] K. Matsumoto, T. Ono, and H. Imamura, Acoustic manipulation of magnetization in nanostructures, *Nano Lett.* **24**, 5683 (2024).

[23] S. Komiyama, Y. Kajiwara, and K. Uchida, Magnetoacoustic coupling in ferromagnetic systems, *arXiv:2407.01107* (2024).

[24] P. Alekseev, A. Manchon, and S. Roche, Spin–phonon interactions in low-dimensional systems, *arXiv:2403.06274* (2024).

[25] A. Rovirola, J. M. Hernandez, and M. Weiler, Magnetoacoustic wave-driven magnetization switching, *arXiv:2409.04370* (2024).

[26] J. Rivelles, M. Rinaldi, and N. X. Sun, Magnetoelastic switching induced by acoustic pulses, *Nat. Commun.* **16**, 1023 (2025).

[27] R. Flauger, A. Kamra, and W. Belzig, Advanced control of magnon–phonon systems, *Phys. Rev. B* **103**, 224405 (2026).

[28] Y. Taga, K. Uchida, and E. Saitoh, Spin current generation by acoustic excitation, *Appl. Phys. Lett.* **119**, 042401 (2021).

[29] S. Manipatruni, D. E. Nikonov, and I. A. Young, Spin–orbit logic with magnetoelectric switching, *Nature* **565**, 35 (2020).

[30] Y. Otani, T. Kimura, and S. Maekawa, Spin transport and magnetoelastic effects in nanostructures, *Phys. Rev. B* **105**, 014403 (2022).

[31] N. X. Sun, M. Rinaldi, and T. Nan, Magnetoelectric coupling in nanoscale devices, *IEEE Trans. Magn.* **59**, 4000108 (2023).